This is the author-created version of the following work:

Boyle, G.J., McEachran, R.P., Cocks, D.G., and White, R.D. (2015) *Electron scattering and transport in liquid argon.* **Journal of Chemical Physics, 142 (15) pp. 1-12.**

Access to this file is available from:

https://researchonline.jcu.edu.au/41918/

Please refer to the original source for the final version of this work:

http://dx.doi.org/10.1063/1.4917258

Electron scattering and transport in liquid argon

G. J. Boyle,[1] R. P. McEachran,[2] D. G. Cocks,[1] and R. D. White[1]

[1]*College of Science, Technology & Engineering,*

James Cook University, Townsville 4810, Australia

[2]*Research School of Physical Sciences and Engineering,*

Australian National University, Canberra, ACT 0200, Australia

Abstract

The transport of excess electrons in liquid argon driven out of equilibrium by an applied electric field is revisited using a multi-term solution of Boltzmann's equation together with ab initio liquid phase cross-sections calculated using the Dirac-Fock scattering equations. The calculation of liquid phase cross-sections extends previous treatments to consider multipole polarisabilities and a non-local treatment of exchange while the accuracy of the electron-argon potential is validated through comparison of the calculated gas phase cross-section with experiment. The results presented highlight the inadequacy of local treatments of exchange that are commonly used in liquid and cluster phase cross-section calculations. The multi-term Boltzmann equation framework accounting for coherent scattering enables the inclusion of the full anisotropy in the differential cross-section arising from the interaction and the structure factor, without an a priori assumption of quasi-isotropy in the velocity distribution function. The model, which contains no free parameters and accounts for both coherent scattering and liquid phase screening effects, was found to reproduce well the experimental drift velocities and characteristic energies.

I. INTRODUCTION

The study of electron transport in non-polar liquids is of fundamental interest for understanding the dynamics of electronic processes in liquids and disordered systems, including dynamic and scattering processes. More recently, attention has focussed on applications including liquid state electronics, driven by use in high-energy particle detectors such as the liquid argon time projection chamber (LArTPC). Advances in the fields of plasma discharges in liquids and associated electrical breakdowns (see e.g. the review of Bruggmen [1]) are dependent on a fundamental knowledge of charged particle transport in liquids. Furthermore, the rapidly developing interdisciplinary field of plasma medicine requires [2–5] a detailed knowledge of electron transport through liquid water and other biostructures, typically under non-equilibrium conditions.

The study of excess electrons in dense gases and fluids is a complex problem, requiring the inclusion of many effects that are not present in dilute gaseous systems. The major contributions to these effects arise from the small interparticle spacings and their highly correlated separations. For thermal energies, the de Broglie wavelengths of the excess electrons are often orders of magnitude larger than the interatomic spacing, which leads to significant quantum-like effects. Even within a semi-classical picture, where the excess electrons are assumed to act as point-like particles, no particular volume is "owned" by a single atom. This means the typical picture for transport in a gas, i.e. a series of individual collision events separated by the mean-free path, is no longer valid, making it important to consider multiple scattering effects of the electron from many atoms simultaneously. Of particular note is the effect of "coherent scattering" and the pair correlations of the liquid play a very important role in this and other effects.

Many previous calculations for electrons in dense systems have neglected these liquid effects for simplicity, modelling dense fluids by applying a theory for dilute gases with only an appropriate increase of the density. However, a few alternative theories exist that have explored liquids in different ways. Borghesani et al [6] have heuristically combined the liquid effects identified above to obtain an effective cross-section. When used in the standard equations from kinetic theory for mobility in a non-zero field, their results have been shown to be remarkably accurate. Braglia and Dallacasa [7] have derived a theory that addresses both enhancements and reductions to the zero-field mobility through a Green's function

approach with appropriate approximations to the self-energy but do not go beyond linear response theory and hence do not explain non-equilibrium behaviour at high fields.

In contrast to the above approaches, the seminal articles by Lekner and Cohen [8, 9] outline a method to address effects of a dense fluid from an ab initio approach by appropriate modifications of the microscopic processes. The article by Lekner [9] describes how an effective potential for a single collision event can be built up from knowledge of only the single-atom/electron potential and the pair correlator of the fluid as well as prescribing a method for obtaining effective cross-sections from this potential. The article by Cohen and Lekner [8] then describes how the effects of coherent scattering can be included with these effective cross-sections in a Boltzmann equation solution for the calculation of transport properties. Sakai et al [10] have been able to improve agreement with experiment by empirically modifying the resultant cross-sections of the Cohen and Lekner formalism and by including inelastic processes. Atrazhev et al [11] were able to simplify the arguments of Lekner [9] to argue that, for small energies, the effective cross-section becomes dependent on the density only and obtained good agreement with experiment. However the distance at which to enforce this new behaviour of the effective cross-section remains a free parameter in the theory and this constant effective cross-section must be found empirically. Atrazhev and co-workers went on to consider the interaction as a muffin tin potential, with each cell being a Wigner-Seitz sphere surrounding each atom in the liquid. They used a variable phase function method which could describe the absence of a Ramsauer minimum in the liquid cross-section along with density fluctuations of the liquid [12–14].

The calculations we present in this paper are based on a generalization of the Cohen and Lekner formalism, overcoming several approximations which are no longer necessary in modern day transport and scattering theory. With regard to the scattering potential, Lekner [9] used the Buckingham potential [15] as input, which we will show is completely inadequate due to its omission of the exchange interaction. This is not noticeable for gas phase measurements, due to the fitting parameter of the Buckingham potential, but shows significant differences after the liquid modifications are applied. By performing a detatiled analysis of the partial phase shifts, Atrazhev and co-workers [13] were able to isolate the important properties of the potential which are required for accurate determination of the transport properties. Our calculations instead avoid these difficulties by using accurate forms for the electron-atom interaction.

With regard to the transport theory itself, we employ a previously derived extension of the Cohen and Lekner formalism for the Boltzmann equation from a two-term to a full multiterm treatment of the velocity distribution function [16]. This theory utlises the full anisotropic detail of the cross-sections that is available in our calculations. For dilute gaseous systems, the two-term approximation can be in serious error [17], and in this study we consider contributions to the error arising from the neglect of the full anisotropy in both the velocity distribution function and the differential scattering cross-section for liquid systems. We perform calculations specifically for the noble gas of argon, which is an excellent test bed for new theories due to the good availability of experimental data and the high degree of accuracy to which ab initio calculations can model the gaseous phase. Available experimental data include drift velocities and characteristic energies in both the gas and liquid phases, as well as precise single-atom cross-sections. We emphasize that we are interested in the full non-equilibrium description of the transport properties and not only that of zero-field mobilities, and so we must consider the full range of the static structure factor $S(K)$ instead of $S(0)$ which is fixed by the isothermal compressibility.

In the following sections we consider the calculation of the macroscopic swarm transport properties in the gaseous and liquid environments from the microscopic cross-sections, modified by the screening and coherent scattering effects discussed above. We first detail the calculation of the gas phase cross sections in section II, using accurate potentials in the Dirac-Fock scattering equations and then address, in section III, effects of screening in the liquid. The transition from a gas to liquid requires a modification of the scattering to include an effective scattering potential and an effective non-local exchange term which we describe in section IV. The application of these cross sections in structured media is outlined in section V and we present the results of our transport calculations in section VI. Initially in Section VI A we consider only the gas phase, understanding the importance of an accurate treatment of exchange and polarization and thereby establishing the credibility of the initial gas-phase potential subsequently used as input for the calculation of cross-sections for the liquid phase environment. Transport coefficients calculated using the screened cross-sections and associated coherent scattering effects are considered in Section VI B, where they are compared with the available measured transport data. Throughout this paper we will make use of atomic units ($m = e = a_0 = \hbar = 1$) unless otherwise specified.

II. SCATTERING OF ELECTRONS BY ARGON GAS

The core of a transport calculation is based on an accurate description of the scattering of the electron off a particle in the bulk. Effective interaction potentials are often used to determine various measurable properties, such as scattering lengths or polarizabilities. These effective potentials are successful so long as they correctly reproduce these quantities for input in other simulations. However, as mentioned above, there are many additional effects due to a dense gas or liquid which can modify the details of the scattering processes. Hence, we require a potential that does not only produce the correct scattering properties in the dilute limit but also well describes the scattering properties under a perturbation of the potential.

In the pure elastic energy region, in addition to the static potential, there are only two interactions which need to be taken into account in electron-atom collisions, namely polarization and exchange. The polarization can be accounted for by means of long-range multipole polarization potentials while the exchange interaction is represented most accurately by a short-range non-local potential formed by antisymmetrizing the total scattering wavefunction.

In the present work the scattering of the incident electrons, with wavenumber k, by argon atoms is described in the gaseous phase by the integral formulation of the partial wave Dirac-Fock scattering equations (see [18] for details). In matrix form, these equations can be written as

$$\begin{pmatrix} f_\kappa(r) \\ g_\kappa(r) \end{pmatrix} = \begin{pmatrix} v_1(kr) \\ v_2(kr) \end{pmatrix} + \frac{1}{k} \int_0^r dx\, G(r,x) \left[U(x) \begin{pmatrix} f_\kappa(x) \\ g_\kappa(x) \end{pmatrix} - \begin{pmatrix} \overline{W}_Q(\kappa;x) \\ \overline{W}_P(\kappa;x) \end{pmatrix} \right], \qquad (1)$$

where the local potential $U(r)$ is given by the sum of the static and local polarization potentials i.e.,

$$U(r) = U_{\rm s}(r) + U_{\rm p}(r) \qquad (2)$$

and $\overline{W}_P(\kappa;r)$ and $\overline{W}_Q(\kappa;r)$ represent the large and small components of the exchange interaction. In equation (1), $f_\kappa(r)$ and $g_\kappa(r)$ are the large and small components of the scattering wavefunction where the quantum number κ can be expressed in terms of the total

and orbital angular momentum quantum numbers j and l according to

$$j = |\kappa| - \frac{1}{2} \quad \text{with} \quad l = \begin{cases} \kappa, & \text{if } \kappa > 0 \\ -\kappa - 1, & \text{if } \kappa < 0 \end{cases} . \tag{3}$$

The free particle Green's function $G(r, x)$ in equation (1) is defined in terms of Riccati-Bessel and Riccati-Neumann functions (see equations (23) and (24a,b) of ref. [18]). The kinetic energy ϵ of the incident electron and its wavenumber k are related by

$$k^2 = \frac{1}{\hbar^2 c^2} \epsilon \left(\epsilon + 2mc^2 \right) . \tag{4}$$

We note that if we ignore ϵ with respect to $2mc^2$, we obtain the usual non-relativistic relationship between the wavenumber and the energy of the incident electron.

The static potential $U_{\mathrm{s}}(r)$ in equation (2) is determined in the usual manner from the Dirac-Fock orbitals of the atom [18]. The polarization potential $U_{\mathrm{p}}(r)$ was determined using the polarized orbital method [19] and contained several static multipole terms as well as the corresponding dynamic polarization terms [20, 21]. In total, the potential $U_{\mathrm{p}}(r)$ contained all terms up to and including those that behave as r^{-14} asymptotically.

Finally, the exchange terms $\overline{W}_P(\kappa; r)$ and $\overline{W}_Q(\kappa; r)$ in equation (1) are given by

$$\overline{W}_{P \text{ or } Q}(\kappa_2; r) = (1 + \gamma) \sum_{n'\kappa'} \{ P_{n'\kappa'}(r) \text{ or } Q_{n'\kappa'}(r) \} \{ - \left[\epsilon_{n'\kappa'} + \epsilon \right] \Delta_{n'\kappa'} \delta(\kappa, \kappa')$$
$$+ e^2 \sum_{\nu} q_{n'\kappa'} \frac{1}{2\nu + 1} C^2(j\, j'\, \nu; -\tfrac{1}{2}\, \tfrac{1}{2}) \frac{1}{r}\, y_{\nu}(n'\kappa', \kappa; r) \} \tag{5}$$

Here, $C(j\, j'\, \nu; -\tfrac{1}{2}\, \tfrac{1}{2})$ is the usual Clebsch-Gordan coefficient and the sum over $n'\kappa'$ in equation (5) is over the atomic orbitals of the ground state while $q_{n'\kappa'} = 2j' + 1$ is the occupation number of these closed sub-shells where the $\epsilon_{n'\kappa'}$ are the eigenvalues of these sub-shells. The exact form of the definite integral $\Delta_{n'\kappa'}$ and the indefinite integral $r^{-1}\, y_{\nu}(n'\kappa', \kappa; r)$ are given in equations (11) and (12) of ref. [22].

We note that the dependence of the exchange terms (5) on the wave function requires an iterative solution for equation (1).

In the integral equation formulation, the scattering phase shifts can be determined from the asymptotic form of the large component of the scattering wavefunction i.e.,

$$f_\kappa(r) \xrightarrow[r \to \infty]{} A_\kappa\, \hat{\jmath}_l(kr) - B_\kappa\, \hat{n}_l(kr) , \tag{6}$$

6

where

$$A_\kappa = 1 - \frac{1}{k} \int_0^\infty \mathrm{d}r \left\{ \bar{v}_1(kr) \left[U(r) f_\kappa(r) - \overline{W}_P(\kappa; r) \right] + \bar{v}_2(kr) \left[U(r) g_\kappa(r) - \overline{W}_Q(\kappa; r) \right] \right\} \quad (7)$$

and

$$B_\kappa = -\frac{1}{k} \int_0^\infty \mathrm{d}r \left\{ v_1(kr) \left[U(r) f_\kappa(r) - \overline{W}_P(\kappa; r) \right] + v_2(kr) \left[U(r) g_\kappa(r) - \overline{W}_Q(\kappa; r) \right] \right\}. \quad (8)$$

The partial wave phase shifts are then given by

$$\tan \delta_l^\pm(k) = \frac{B_\kappa}{A_\kappa}, \quad (9)$$

where the $\delta_l^\pm$ are the spin-up $(+)$ and spin-down $(-)$ phase shifts.

The total elastic and momentum transfer cross-sections are given, in terms of these phase shifts, by

$$\sigma_{\mathrm{el}}(k^2) = \frac{4\pi}{k^2} \sum_{l=0}^\infty \left\{ (l+1) \sin^2 \delta_l^+(k) + l \sin^2 \delta_l^-(k) \right\} \quad (10)$$

and

$$\sigma_{\mathrm{mt}}(k^2) = \frac{4\pi}{k^2} \sum_{l=0}^\infty \left\{ \frac{(l+1)(l+2)}{2l+3} \sin^2\left(\delta_l^+(k) - \delta_{l+1}^+(k)\right) + \frac{l(l+1)}{2l+1} \sin^2\left(\delta_l^-(k) - \delta_{l+1}^-(k)\right) \right.$$

$$\left. + \frac{(l+1)}{(2l+1)(2l+3)} \sin^2\left(\delta_l^+((k) - \delta_{l+1}^-(k)\right) \right\} \quad (11)$$

which can be shown to reduce to the non-relativistic results if we set $\delta_l^+(k) = \delta_l^-(k) = \delta_l(k)$.

As can be seen in Figure 1, neither the polarization nor the exchange interaction alone is capable of reproducing the true Ramsauer minimum in the argon momentum transfer cross-section; it is only when we combine these two interactions that there is agreement with experiment. This is also true for the Ramsauer minimum in the elastic cross-section.

In the original work of [9], Lekner described the elastic scattering of electrons by argon atoms by just the local dipole polarization potential of Buckingham [15] which is given by

$$U_{\mathrm{p}}(r) = -\frac{\alpha_{\mathrm{d}}}{2 \left(r^2 + r_a^2\right)^2}, \quad (12)$$

where α_{d} is the static dipole polarizability of argon and r_a is an adjustable parameter. Lekner chose this parameter so as to obtain the experimental scattering length $a_0 = -1.5$ a.u. of [23].
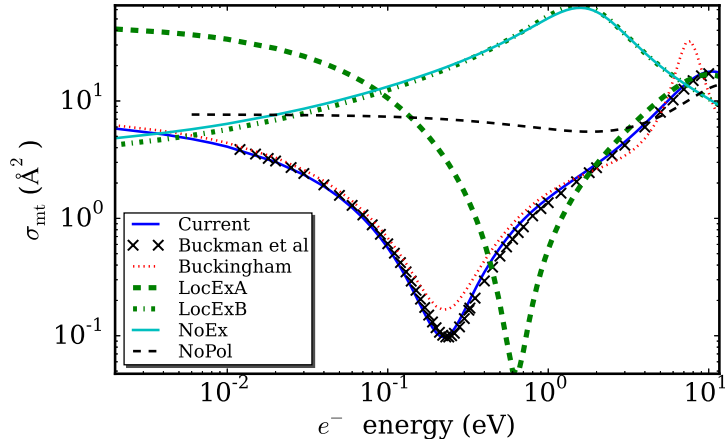
7

Figure 1. Cross-sections for electron scattering from argon. The calculations described in this paper, which use the non-local exchange interaction (solid line) are in good agreement with the recommended set of Buckman et al. [24]. A comparison with a calculation similar to that of Lekner [9] using a Buckingham potential (dotted line) shows loose qualitative agreement at the Ramsauer minimum, but quantitatively is incorrect. Also shown are the results from using two different effective models of a local exchange potential (thick dashed [25] and dash-dotted lines [26]) which do not agree with experimental measurement at all, as well as the cross-section when exchange is included but polarization is neglected (thin dashed line).

This value is very close to the current recommended value of $a_0 = -1.45$ a.u. of [24]. The value obtained in the current work is $a_0 = -1.46$ a.u.

As a consequence of Lekner's choice for the adjustable parameter r_a, his simple polarization potential in equation (12) was able to mimic the effects of both the polarization and exchange interactions at low energies of the incident electron and his calculation was able to produce a low-energy Ramsauer minimum in the momentum transfer cross-section. At higher energies his momentum transfer cross-section deviates from the experimental cross-section.

We show our cross-sections calculated using (10) in Figure 1. We obtain very good agreement with the recommended set of cross-sections of [24] which combine many different experimental measurements and theoretical calculations. In order to demonstrate the importance of including the non-local exchange interaction, we have also repeated the calculation using two different model potentials that replace the non-local exchange with an effective

local term in the potential [25, 26]. One of these local approximations [25] is qualitatively wrong, showing the same behaviour as that without exchange. The other approximation [26] is qualitatively similar but differs in the scattering length and position of the Ramsauer minimum by an order of magnitude. It is clear to see that there is a significant difference between the results. When we compare our results to those of the Buckingham potential, where we set $r_\alpha = 1.087$ a.u. such that the scattering length is $a_0 = -1.50$ a.u., we find that it does follow the general shape of the Ramsauer minimum. However, we emphasize that this is a result of the fitting parameter r_α and this potential does not accurately describe the details of the scattering.

III. SCREENING OF THE POLARIZATION INTERACTION

The effects of the high density of the liquid are included in our calculations by several modifications of the gas scattering properties. The first of these is to account for the screening of a single induced atomic dipole by the induced dipoles of all other atoms. Our procedure outlined in this section closely follows that of Lekner [9].

In the dilute gas limit, the mobile electron undergoes a collision with a single atom of the gas effectively in isolation from all other atoms in the gas. During this collision the electron induces a set of multipole moments in the atom, which in turn interact with the electron through a charge-multipole potential, resulting in the polarization potential, $U_\mathrm{p}(r)$, of section II above. For a dilute gas, the range of the potential produced by these induced multipole moments is relatively small compared with the large interatomic spacing and so it is a good approximation to neglect their effect on other atoms. However, with higher densities of the gas or liquid, many atoms can have a non-negligible induced set of multipole moments originating from both the mobile electron and from all other atoms in the bulk. The effective charge-multipole polarization potential felt by the electron at any particular location $\boldsymbol{r}_e$ is then the sum of the polarization potentials from all atoms.

We consider effects originating from the induced dipoles of the atoms only and determine the effective polarization of an individual atom self-consistently. We first assume that the induced dipole strength for every atom in the bulk can be written as $f(r)\alpha_d(r)e/r^2$ where r is the distance of the electron from the atom, $\alpha_d(r)$ is the exterior dipole polarizability (see [27], equation (1)) for a single atom that results from the interaction with the electron, and $f(r)$

accounts for polarization screening which must be determined. This simple multiplicative factor is valid, so long as we average over the atomic distribution. In the dilute-gas limit, we can safely approximate $f(r) = 1$, and in the dense case we must obtain a self-consistent expression for $f(r)$. By choosing a particular "focus atom" i at location $\boldsymbol{r}_i$ such that $\boldsymbol{r} = \boldsymbol{r}_e - \boldsymbol{r}_i$, and assuming that the coefficient $f(r)$ is known for all other atoms, which we denote by $f_{\text{bulk}}(r)$, we can calculate [9] the dipole strength for atom i from:

$$f_i(r) = 1 - \pi N \int_0^\infty ds \, \frac{g(s)}{s^2} \int_{|r-s|}^{r+s} dt \, \Theta(r,s,t) \frac{\alpha_d(t) f_{\text{bulk}}(t)}{t^2} \tag{13}$$

which has been obtained using bipolar coordinates, s and t, where N is the density of the bulk, $g(s)$ is the isotropic pair correlator of the bulk and the factor

$$\Theta(r,s,t) = \frac{3}{2} \frac{(s^2 + t^2 - r^2)(s^2 + r^2 - t^2)}{s^2} + (r^2 + t^2 - s^2), \tag{14}$$

arises due to the form of the electric field of a dipole. The integrations over s and t represent the contribution from an atom located at a distance s from atom i and a distance t from the electron. The likelihood of finding an atom is determined by $g(s)$ and so it can be seen that equation (13) approximates the exact polarization by that resulting from the ensemble average of all atomic configurations, given that one atom is located at $\boldsymbol{r}_i$. In this approximation, the polarization itself is always aligned along the vector $\hat{\boldsymbol{r}}$ between the focus atom and the electron.

The self-consistent solution to equation (13) is obtained by setting $f_i(r) = f_{\text{bulk}}(r)$ and solving for $f_i(r)$, which we do by iteration. The most important quantity in equation (13) is the pair correlator, which represents the next order in the particle distribution in the bulk beyond the average density. In the calculation of Lekner, the pair correlator was taken to be the analytical solution of the Percus-Yevick model for ease of calculation. In our calculation, we go beyond this by using the experimental measurements of Yarnell [28] to more accurately describe the correlations. The data we use, which was obtained for a bulk density of $N = 0.0213 \, \text{Å}^{-3}$, is shown in Figure 2 and compared with the Percus-Yevick model at the same density.

Using the pair correlator of argon, we have self-consistently calculated the screening function $f(r)$ and show the result in Figure 3. Although this screening factor technically applies to the dipole term only, we work with a rather more complicated form of the polarization term than Lekner had originally considered. However, as the largest contribution to the
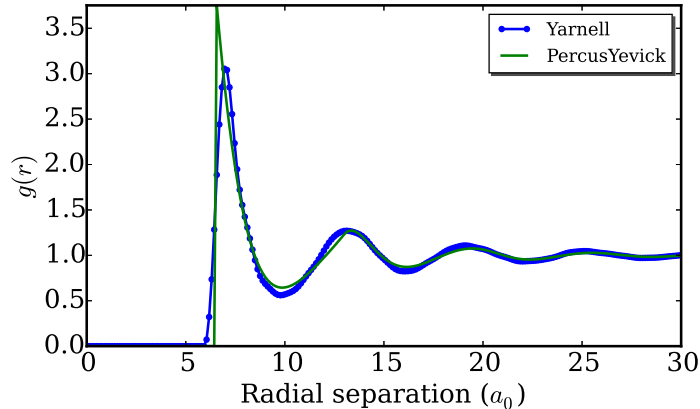
Figure 2. Pair correlator for argon, as reported in Yarnell [28], measured in neutron scattering experiments. Also plotted, is the pair correlator calculated in the analytical Percus-Yevick approximation as used by Lekner [9].

polarization does indeed come from the dipole term, we have decided to apply the screening factor $f(r)$ to the entire polarization potential. Hence, with the screening of the polarization taken into account, the screened polarization potential, $\tilde{U}_p(r)$, of an electron with one atom in a dense fluid is given by:

$$\tilde{U}_p(r) = f(r)U_{\mathrm{p}}(r) \ . \tag{15}$$

We note that, in contrast to Lekner, who used only the static dipole polarizability α_d, the more accurate representation of the atom-electron interaction as described in section II has already led to a radial dependence of the polarization potential $U_p(r)$ beyond that of a potential whose asymptotic behaviour is r^{-4}. The effect of the screening has hence led to a further modification of $U_p(r)$ which is density dependent.

IV. EFFECTIVE POTENTIAL IN LIQUID

For input into the kinetic theory, we require appropriate cross-sections for the scattering of the electron from a single "focus atom" in the bulk. As discussed above, the presence of the other atoms screens the polarization interaction between the electron and the focus atom. However, there is another more obvious effect resulting from the other atoms in the bulk: their interaction with the electron itself remains significant even when the electron
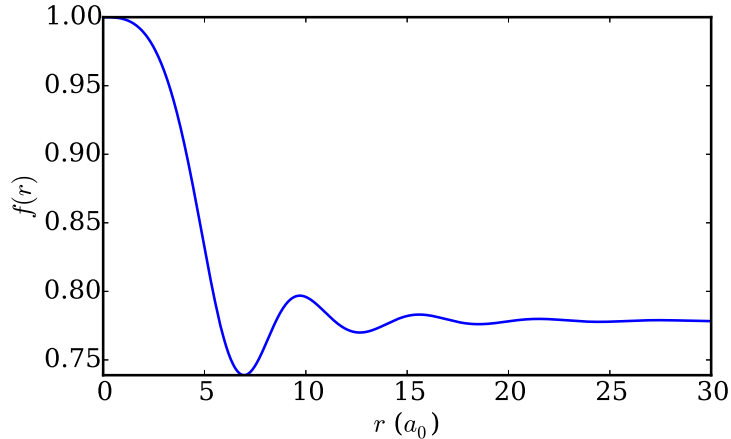
11

Figure 3. The screening function $f(r)$ of the polarization interaction potential for scattering of an electron from a single argon atom in a bulk of density $N = 0.0213\,\text{Å}^{-3}$.

is very close to the focus atom. Hence, as outlined in Lekner [9], we build up an effective potential that is experienced by the electron throughout a single scattering event, as well as define what is meant by "a single scattering event". Although we follow the general principles of [9], we calculate the cross-sections in a distinctly different fashion.

The effective potential that we consider $U_{\text{eff}} = U_1 + U_2$ is made of two parts: $U_1(r)$ which corresponds to the direct interactions with the focus atom, and $U_2(r)$, which corresponds to the interaction of the electron with the rest of the bulk. As it is prohibitively expensive to treat exact configurations of atoms in the bulk, we build the external potential U_2 by again taking the ensemble average:

$$U_2(r) = \frac{2\pi N}{r} \int_0^\infty dt\, U_1(t) \int_{|r-t|}^{r+t} ds\, sg(s) \,, \tag{16}$$

where the order of integration has been reversed in comparison to (13) for numerical convenience [44]. We note that taking the ensemble average has the advantage of enforcing spherical symmetry of the total effective potential U_{eff}. In calculating (13) and (16), we make use of the quantity σ_{core}, which corresponds to the hard-core exclusion diameter for the distribution of atoms in the bulk, i.e. the probability for two atoms to approach within a distance σ_{core} is vanishingly small. For argon $\sigma_{\text{core}} \approx 6\,a_0$ and we take advantage of this by explicitly setting $g(s) = 0$ for $s < \sigma_{\text{core}}$ and adjusting the limits of equations (13) and (16) accordingly.

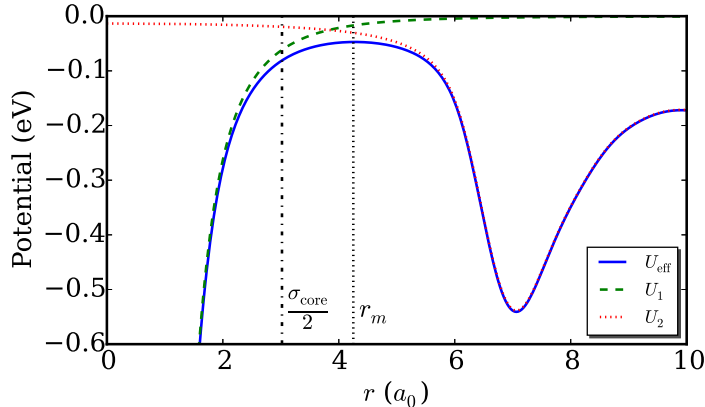In addition we go beyond Lekner's calculation by including the effects of the exchange

12

Figure 4. Plots of the total effective potential U_{eff} felt by an electron when colliding with one atom in the liquid. Also shown are the components, U_1 and U_2, which represent the direct potential of the atom and the contribution of the remaining atoms in the bulk respectively. The dashed vertical lines at $\sigma_{\text{core}}/2$ and r_m indicate the hard-core exclusion radius and the proposed collisional sphere respectively. Note that effects of exchange are not represented in this figure.

terms in the bulk. We do this by performing the same ensemble average as in (16) but over the quantities $\overline{W}_P$ and $\overline{W}_Q$ instead of U_1, obtaining bulk averages $\overline{W}_{P,2}$ and $\overline{W}_{Q,2}$. These are then included as effective exchange terms, $\overline{W}_{(P \text{ or } Q),\text{eff}} = \overline{W}_{P \text{ or } Q} + \overline{W}_{(P \text{ or } Q),2}$ in the Dirac-Fock scattering equations (1). In contrast to U_2, these exchange terms are dependent on the wave function itself, so the ensemble averages must be recalculated at every iteration in the solution of (1).

A plot of the functions U_{eff}, U_1 and U_2 is shown in Figure 4. It can be seen that there is a turning point that occurs at a distance we denote by r_m. In the dense gas limit that we are investigating, this value is $r_m \approx 4.3\,a_0$. The turning point at r_m provides a natural distinction between the volume that is under the influence of the focus atom, i.e. the sphere of radius r_m, and that of the rest of the bulk. Hence, we can say that a single collision event takes place when an electron enters and leaves the radius r_m of a single atom. We note that $r_m \approx \frac{2}{3}\sigma_{\text{core}} > \sigma_{\text{core}}/2$, i.e. r_m is larger than half of the minimal interatomic separation, which could be considered to define the volume "owned by" the focus atom and hence a logical choice for the "collision event radius". r_m is also different from the Wigner-Seitz diameter $d_{\text{WS}} = 2(4\pi N/3)^{-1/3} \approx 4.2\,a_0$ [14], although it is very similar.

We would now like to solve for the scattering properties, in particular the cross-sections,

13

from such a collision process. We assume that it remains reasonable to extract the cross-sections through the phase shifts in a partial wave equation. In order to determine these, Lekner chose to shift the effective potential by an amount U_0 such that $U_{\text{eff}}(r_m) + U_0 = 0$, and to set the potential $U_{\text{eff}}(r > r_m) = 0$, and finally matched to the asymptotic form of each partial wave in the usual fashion. In contrast, we choose to leave the potential unaltered, but calculate the phase shift at the point r_m instead, effectively setting the upper limits of equations (7) and (8) to be r_m instead of infinity. We note that this is also known as calculating the "phase function" [13] at the point r_m, which is equivalent to setting $U_{\text{eff}}(r > r_m) = 0$ and matching to the asymptotic form of the wave function. We believe that this more accurately represents the available energy states in the bulk. We denote this cross section, including external contributions and screening effects, by $\sigma^{\text{scr}}(\epsilon, \chi)$.

As we may assume $g(s) = 0$ for $s < \sigma_{\text{core}}$ and because we calculate the potential only up to a distance of $r_m \approx \frac{2}{3}\sigma_{\text{core}}$, we can see that the integral over t in (16) is non-zero only for $t \gtrsim \frac{1}{3}\sigma_{\text{core}} \approx 2\,a_0$. At these ranges, the dominant contribution to the potential comes from the polarization component. We also note that the values of $\overline{W}_{P,2}$ and $\overline{W}_{Q,2}$ are not well behaved for larger distances and so we set them to be zero for $r > \sigma_{\text{core}}/2$. We have performed calculations that neglect the contribution of $\overline{W}_{P,2}$ and $\overline{W}_{Q,2}$ to the bulk and compared these to the full calculations, which showed very little difference in the high energy regime of the resultant cross-sections and a small difference of up to 5% otherwise. The effect of this change on the transport properties was a small but non-negligible deviation.

A.   Cross-sections and variation of r_m

The choice of the value for r_m is a crucial part of our calculation. It is worth mentioning that the choice we make above is consistent in the limit of $N \to 0$; in this case U_2 is so weak that it is only after U_1 has significantly decayed for very large values of r that $d(U_1 + U_2)/dr = 0$. Hence, $r_m \to \infty$ as $N \to 0$ and our calculation reduces to the usual scattering calculation from a single atom. However, in the dense case, it is not known whether $d(U_1 + U_2)/dr|_{r_m} = 0$ is the best choice to model the scattering in the liquid. Hence, we have also performed a sensitivity analysis on the parameter r_m. We denote the distance at which we calculate the phase shifts by r^* and allow it to vary from our initial choice of $r^* = r_m$. The resultant cross-sections from a variation of $\pm\frac{1}{16}a_0$ are shown in Figure 5 as well as the
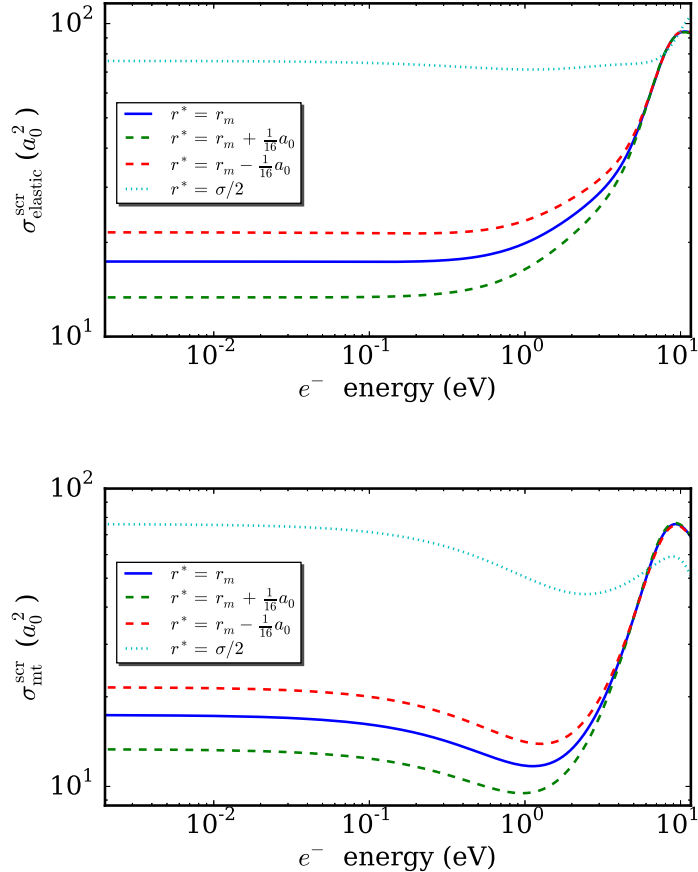
14

Figure 5. Screened elastic total and momentum-transfer cross-sections for argon calculated from the phase shifts determined at a distance r^*. Our preferred choice for transport calculations in this paper, $r^* = r_m$, corresponds to the solid line, the dashed lines are those corresponding to a variations $r^* = r_m \pm \frac{1}{16}a_0$ and the dotted line corresponds to a variation of $r^* = \sigma_{\text{core}}/2$.

more straightforward choice of $r^* = \sigma_{\text{core}}/2$. We note that Atrazhev et al [14] have implicitly investigated this variation previously, in order to describe the effect of density fluctuations on the effective cross-sections. In their case, the value of r^* was set to be the Wigner-Seitz cell radius, which itself depends on the density of the liquid. In contrast, we keep the density fixed while varying r^*.

It can easily be seen that the largest modification to the cross-sections due to the variation in r_m occurs at low energies. Importantly, the more obvious choice of $r^* = \sigma_{\text{core}}/2$ yields a dramatically different behaviour. As will be shown later, the effect that these variations have on the transport measurements is significant and shifts the peak observed in various

transport properties.

We note that we neglect the effect of density fluctuations, which would modify the effective cross-section for the liquid. This was investigated by Atrazhev et al [14], and shown to have a significant contribution to the cross-sections. However, their article focused on a density for which the effective liquid cross-section vanishes, causing the density fluctuations to be the largest contribution for small electron energies. In our case, we can expect density fluctuations to cause both enhancements and reductions of the cross-sections, which would cancel out on average.

V. KINETIC THEORY AND TRANSPORT PROPERTIES

A. Multi-term solution of Boltzmann's equation

The behaviour of electrons in gaseous and liquid argon, driven out of equilibrium via an electric field E, can be described by the solution of the Boltzmann's equation for the phase-space distribution function $f(\boldsymbol{r}, \boldsymbol{v}, t)$ [30]:

$$\frac{\partial f}{\partial t} + \boldsymbol{v} \cdot \nabla f + \frac{e\boldsymbol{E}}{m_e} \cdot \frac{\partial f}{\partial \boldsymbol{v}} = -J(f), \tag{17}$$

where $\boldsymbol{r}$, $\boldsymbol{v}$ and e denote the position, velocity and charge of the electron respectively. The collision operator $J(f)$ accounts for interactions between the electrons of mass m_e and the background material. We restrict our considerations in this study, to those applied reduced electric fields E/N (where N is the number density of the background material) such that no internal states of the individual argon atoms are excited.

To calculate the drift and diffusion coefficients, we represent the spatial dependence of the distribution functions as [31, 32]:

$$f(\boldsymbol{r}, \boldsymbol{v}, t) = F(\boldsymbol{v}, t)n(\boldsymbol{r}, t) - F^{(L)}(\boldsymbol{v})\frac{\partial n}{\partial z} - F^{(T)}(\boldsymbol{v}) \left[\cos\phi\frac{\partial n}{\partial x} + \sin\phi\frac{\partial n}{\partial y}\right] + ..., \tag{18}$$

where the superscripts L and T define quantities that are parallel and transverse to the electric field (defined to be in the z direction) respectively. Solution of Boltzmann's equation (17) requires decomposition of the coefficients in velocity space through an expansion

16

in (associated) Legendre polynomials:

$$F(\boldsymbol{v}) = \sum_{l=0}^{\infty} F_l(v) P_l(\cos\theta)$$

$$F^{(T)}(\boldsymbol{v}) = \sum_{l=0}^{\infty} F_l^{(T)}(v) P_l^1(\cos\theta) , \qquad (19)$$

where θ denotes the angle relative to the electric field direction (taken to be the z-axis). This is a true multi-term solution of Boltzmann's equation, whereby the upper bound in each of the l-summations are truncated at a value $l_{\max}$, and this value is incremented until some convergence criteria is met on the distribution function or its velocity moments. By setting $l_{\max} = 1$ yields the two-term approximation commonly used in all electron transport theory in liquids [6, 8, 10], which enforces a quasi-isotropic distribution. The current theory does not make the quasi-isotropic assumption for the velocity distribution function a priori. By using the orthogonality of (associated) Legendre polynomials, the following hierarchy of equations must be solved to calculate the drift velocity and diffusion tensor [32]:

$$J^l F_l + \frac{l+1}{2l+3} a \left(\frac{\partial}{\partial v} + \frac{l+2}{v} \right) F_{l+1} + \frac{l}{2l-1} a \left(\frac{\partial}{\partial v} - \frac{l-1}{v} \right) F_{l-1} = 0 \qquad (20)$$

$$J^l F_l^{(T)} + \frac{l+2}{2l+3} a \left(\frac{\partial}{\partial v} + \frac{l+2}{v} \right) F_{l+1}^{(T)} + \frac{l-1}{2l-1} a \left(\frac{\partial}{\partial v} - \frac{l-1}{v} \right) F_{l-1}^{(T)} = v \left(\frac{F_{l-1}}{2l-1} - \frac{F_{l+1}}{2l+3} \right) , \qquad (21)$$

where the J^l represent the Legendre projections of the collision operator detailed below and $a = eE/m_e$. The solution of the system of equations (20) and (21) using the collision operator projections (24) and (25) provides sufficient information to calculate the drift velocity W via:

$$W = \frac{4\pi}{3} \int_0^{\infty} v^3 F_1 dv, \qquad (22)$$

and the characteristic energy, defined as the ratio of the transverse diffusion coefficient D_T to the electron mobility $\mu (= W/E)$, via calculation of the transverse diffusion coefficient:

$$D_T = \frac{4\pi}{3} \int_0^{\infty} v^3 F_1^{(T)} dv . \qquad (23)$$

B. Collision operator for interactions in structured matter

The collision operator appearing in (17) describes the rate of change of the distribution function due to interactions with the background material. At low electron energies, where

the de Broglie wavelength of the electron is of the order of the average inter-particle spacing $\sim N^{-1/3}$, the charged particle is best viewed as a wave that is coherently scattered from the various scattering centres that comprise the medium. At higher energies, the de Broglie wavelength becomes much less than the inter-particle spacing and the effects of coherent scattering are no longer important. In this limit, the binary scattering approximation is recovered, although the interaction potential is modified as discussed above. For liquid argon, the average interparticle spacing is approximately $4.5\,\text{Å}$, implying that "low" energies are those less than ~ 7.4 eV, which is several orders of magnitude larger than the thermal energy of ~ 0.01 eV.

Recently, the two-term approximation of Cohen and Lekner [8] was extended to a multi-term regime [16, 33], where the Legendre projections of the collision operator in the small mass ratio limit were shown to be:

$$J^0\left(\Phi_l\right) = \frac{m_e}{Mv^2}\frac{d}{dv}\left\{v\nu_{mt}(v)\left[v\Phi_l + \frac{kT}{m_e}\frac{d}{dv}\Phi_l\right]\right\} \tag{24}$$

$$J^l\Phi_l = \tilde{\nu}_l(v)\Phi_l \qquad \text{for } l{\geq}1, \tag{25}$$

where M is the mass of an argon atom, $\Phi_l = \left\{F_l, F^{(L)}, F^{(T)}\right\}$ and

$$\nu_{mt}(v) = Nv2\pi\int_0^\pi \sigma^{\mathrm{scr}}(v,\chi)\left[1 - P_1(\cos\chi)\right]\sin\chi d\chi = Nv\sigma_{mt}^{\mathrm{scr}}(v), \tag{26}$$

is the binary momentum transfer collision frequency in the absence of coherent scattering effects, while

$$\tilde{\nu}_l(v) = Nv\left(2\pi\int_0^\pi \Sigma(v,\chi)\left[1 - P_l(\cos\chi)\right]\sin\chi d\chi\right), \tag{27}$$

are the structure-modified higher-order collision frequencies. The effects of the structure medium are encapsulated in the static structure factor $S(K)$, which is the Fourier transform of the pair correlator, $g(r)$, used in sections III and IV. The structure factor is included via the term:

$$\Sigma(v,\chi) = \sigma^{\mathrm{scr}}(v,\chi)\,S\left(\frac{2m_ev}{\hbar}\sin\frac{\chi}{2}\right), \tag{28}$$

which represents an effective differential cross-section. If we represent $\Sigma(v,\chi)$ through an expansion in terms of Legendre polynomials:

$$\Sigma(v,\chi) = \sum_{\lambda=0}^{\infty}\frac{2\lambda+1}{2}\Sigma_\lambda(v)P_\lambda\left(\cos\chi\right) \tag{29}$$

18

then one can make connection with the previous calculations of the collision matrix elements for dilute gaseous systems. The effective partial cross-sections $\Sigma_l(c)$ are defined by [16, 33]

$$
\begin{aligned}
\Sigma_l(v) &= 2\pi \int_{-1}^{1} \Sigma(v, \chi) P_l(\cos \chi) d(\cos \chi) \\
&= \frac{1}{4\pi} \sum_{\lambda' \lambda''} \frac{(2\lambda' + 1)(2\lambda'' + 1)}{2l + 1} C^2(\lambda'\,\lambda''\,l; 0\,0) \sigma_{\lambda'}(v) s_{\lambda''}(v),
\end{aligned} \tag{30}
$$

where

$$
\sigma_l(v) = 2\pi \int_{-1}^{1} \sigma^{\text{scr}}(v, \chi) P_l(\cos \chi) d(\cos \chi) \tag{31}
$$

and

$$
s_l(v) = \frac{1}{2} \int_{-1}^{1} S\left(\frac{2m_e v}{\hbar} \sin\left(\frac{\chi}{2}\right)\right) P_l(\cos \chi) d(\cos \chi). \tag{32}
$$

It then follows that

$$
\tilde{\nu}_l(v) = N v \left[\Sigma_0(v) - \Sigma_l(v)\right]. \tag{33}
$$

It is sufficient for this study to consider only low energy coherent elastic scattering processes. At higher fields, incoherent inelastic scattering effects including excitation and ionization would need to be considered [16, 33].

VI.   RESULTS

Swarm experiments are a test of the particle, momentum and energy balance in the cross-section set and the associated transport theory or simulation. In the low-field regime considered in this manuscript, only conservative quasi-elastic processes are operative, and hence the ability of the calculated values of drift and characteristic energy to match the measured coefficients provides this test on momentum and energy balance.

In the following sections we consider the calculation of the macroscopic swarm transport properties in the gaseous and liquid environments from the microscopic cross-sections, including screening and coherent scattering effects as discussed above. Initially in Section VI A we consider only the gas phase, focussing on understanding the importance of an accurate treatment of exchange and polarization and establishing the credibility of the initial gas-phase potential subsequently used as input for the calculation of cross-sections for the liquid

phase environment. Transport coefficients calculated using the screened cross-sections and associated coherent scattering effects are considered in Section VIB, where they are compared with the available measured transport data in the liquid phase.

A. Electrons in gaseous argon – benchmarking the potential and exchange treatment

The calculated drift velocity and characteristic energy transport properties using the gas-phase cross-sections detailed in Section II are presented in Figure 6. They are compared against various experimental data for this gas [34, 35]. We restrict ourselves to the reduced electric fields of less than 3 Td, to ensure we are in the regime where only elastic scattering is operative.

For our current potential, with a non-local treatment of exchange, generally reproduces drift velocities to within the experimental errors. There are small regions of E/N (where the properties vary rapidly with E/N) where errors can be as large 3% in the drift velocity and 10% or the characteristic energy. For the characteristic energy this can be outside the experimental errors in this region. If the exchange interaction is neglected in the calculation of the cross-section, we observe that the calculated values of the transport properties depart from the measured by an order of magnitude or more, reflecting the qualitative disagreement in the form of the cross-sections predicted in Figure 1. Given the similarities in the cross-sections calculated using the local exchange potential B [26] to those neglecting exchange, the calculated transport coefficients are quite similar between the two techniques. Using the local treatment of exchange A [25], which reproduces the Ramsauer minimum in the cross-section (although its depth, location and width disagree quantitatively), the transport coefficients have a similar qualitative form, however they are displaced to significantly higher fields relative to the measured values. As expected, implementation of the Buckingham potential as in Lekner [9], which was tuned to reproduce the zero-energy gas-phase cross-section, produces drift velocities that are accurate to within 10%, however the characteristic energies are significantly worse than those using the current potential.

The results shown here for argon demonstrate the validity of the electron-argon interaction potential developed for the current study, and the necessity for a strict non-local treatment of exchange and an accurate treatment of polarization, in order to generate the accurate
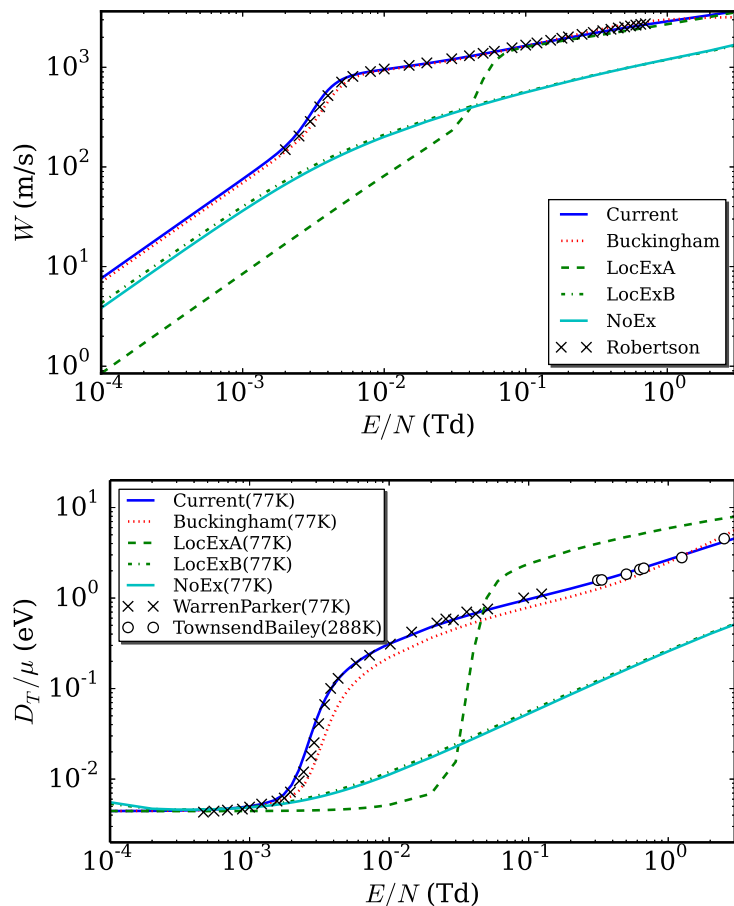
Figure 6. The drift velocity (top) and characteristic energy (bottom) of electrons in gaseous argon, calculated using the potentials and associated cross-sections detailed in Section II, and compared with available experimental data (Robertson [34, 36] at 90 K; Warren and Parker [35, 37] at 77 K; Townsend and Bailey [37, 38] at 288 K). The full non-local treatment of exchange considered here is compared to two forms of local exchange potentials (LocExA [25]; LocExB [26]) and to the case when the exchange interaction is neglected altogether. The background argon gas for the calculations was fixed at 90 K for determination of the drift velocity and 77 K for the characteristic energy.

microscopic differential cross-sections. The small disagreement for the characteristic energy over a small range of E/N may reflect some minor limitations in the cross section data base.

B. Electrons in liquid argon

In Figure 7, we compare the drift velocity and characteristic energies in both the gaseous and liquid phases. The transport coefficients are presented as a function of the reduced electric fields, so that the explicit density dependence has been scaled out and we have a true comparison of the gaseous and liquid phases. For a given reduced field, we observe that the drift velocity in the liquid phase is enhanced by as much as an order of magnitude over the gaseous phase in the reduced field range considered. Contrarily, the characteristic energy in the liquid phase is reduced relative to the gaseous phase by as much as 500% over the range of fields for which the data exists. Importantly, the measured data emphasizes that transport of electrons in liquids cannot be treated by using only the gas phase cross-sections and scaling of the density to those of liquids.

We now assess the importance of including various physical processes present in liquids in reproducing the measured transport coefficients.

Firstly, we assess the importance of coherent scattering effects, by implementing the gas-phase interaction potential and associated cross-sections into the coherent scattering framework detailed in Section V B. The resulting cross-sections are displayed in Figure 8. We observe in Figure 7 that the inclusion of only coherent scattering effects acts to enhance both the drift velocity and the characteristic energy. This is a reflection of the reduced momentum transfer cross-section in Figure 8 in the regime where coherent scattering effects are operative [16]. Interestingly, coherent scattering produces the physical process of negative differential conductivity (i.e. the fall of the drift velocity with increasing electric field) which is absent from the gas-phase calculations, as discussed elsewhere [16]. While the inclusion of coherent scattering effects results in a calculated drift velocity of the same order of magnitude as the experimental data, it does not reproduce the correct shape in the profiles, with errors as large as 250%. Further, the calculated characteristic energy produced by including coherent scattering enhances the characteristic energies relative to the gas phase which is inconsistent with the experimental data.

Secondly, in addition to the coherent scattering, we now include the full liquid induced effects on the potential as detailed in Sections III and IV. The resulting cross-sections are displayed in Figure 8, where we emphasize that such effects act to essentially remove the Ramsauer minimum in the cross-section. This produces an enhanced and relatively constant

22

cross-section in that energy regime. This is very similar to that predicted by Atrazhev and Iakubov [11], in their reduction of the Cohen and Lekner theory, which suggested that a cross-section that is only density dependent would occur for low impact energies. In Figure 7 we demonstrate that the inclusion of both scattering potential modification and coherent scattering produces drift velocities and characteristic energies that are both qualitatively and quantitatively in agreement with the experimental data. Errors in the drift velocities and characteristic energies are significantly reduced.

In Figure 5, we highlighted the sensitivity of the calculated cross-sections in the liquid phase to the value of r^* at which the phase shifts are determined. The macroscopic manifestations of this sensitivity on both the drift velocity and characteristic energy is presented in Figure 9. Slight modifications of r^* by $a_0/16$ from the preferred value of $r^* = r_m$ emphasize the sensitivity of the transport coefficients to this value. The choice of $r^* = \sigma_{\mathrm{core}}/2$ produces results that are essentially translated to higher reduced electric fields. Importantly, these results indicate that the value of r_m may be energy dependent. One could possibly tune the value of r_m to match the experimental data, however we have strived to eliminate adjustable parameters in our formalism. One may also look at using an alternative scheme that is energy-dependent for choosing the value of r_m, e.g. including contributions from the exchange terms $\overline{W}_{P,\mathrm{eff}}$ and $\overline{W}_{Q,\mathrm{eff}}$.

C. Impact of scattering anisotropy and the two-term approximation

We conclude this study by considering the impact of the anisotropy in both the scattering cross-sections and the velocity distribution function on the calculated transport properties.

In Figure 10 we display the differential cross-sections for the gas phase phase and for the liquid modified differential cross-sections, highlighting the impact of coherent scattering effects. For the dilute gas phase, we observe at low energies that the differential cross-sections are small and essentially isotropic. As we move to higher energies, the differential cross-section begins to demonstrate an increased magnitude and also enhanced anisotropy, with peaks in the forward and back-scattering directions. This is confirmed by agreement with the experimental data of Gibson et al. [42]. When we account for liquid effects in the scattering potential, we observe that similar qualitative structures are present in the resulting differential cross-section, with slightly more structure than for the dilute gas
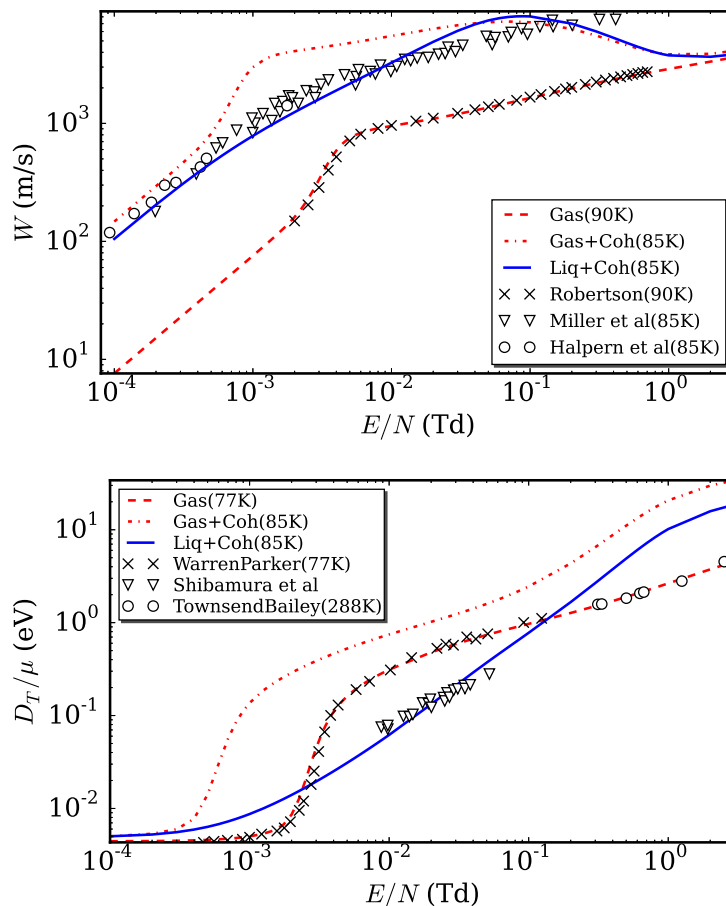
Figure 7. Comparison of the measured drift velocities W and characteristic energies D_T/μ in gaseous and liquid argon, with those calculated from the various approximations to the cross-sections. Experimental data (Robertson [34, 36] at 90 K; Miller et al [39] at 85 K; Halpern et al [40] at 85 K; Warren and Parker [35, 37] at 77 K; Townsend and Bailey [37, 38] at 288 K; Shibamura et al [41] at an unmeasured liquid temperature). The various approximations used are: gas-phase only cross-sections (Gas), gas-phase cross-sections with coherent scattering (Gas+Coh), and liquid phase cross-sections with coherent scattering effects (Liq+Coh). The results have been calculated using the full differential cross-section and results are converged multi-term values. Experimental uncertainties are estimated at 2% for Robertson and less than 15% for Shibamura et al.

phase. When the liquid phase differential cross-section is combined with the structure factor accounting for coherent scattering effects, the resulting differential cross-section $\Sigma(\epsilon, \chi)$ takes on a completely different qualitative structure. The forward peak in the differential cross-section is removed, with suppression of the cross-section at low energies and low scattering
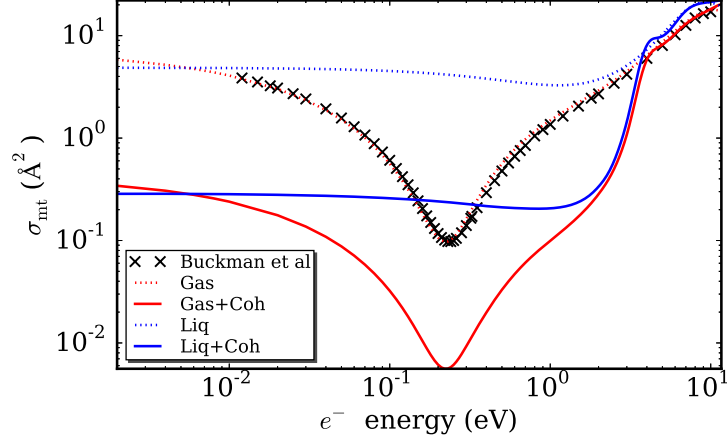
Figure 8. The momentum transfer cross-sections in the gas-phase (Gas), liquid-phase (Liq) and their modifications when coherent scattering effects are included (+Coh). The recommended transfer cross-section of reference [24] for a dilute gas is a combination of experimental measurements and theoretical calculations.

angles. The backscattering peak in the differential cross-section at high energies remains unaffected, while subpeaks in the differential cross-section are enhanced by the coherent scattering effects.

The degree of anisotropy in the distribution function is evidenced by an enhanced value of $l_{\max}$ required in the spherical harmonic expansions (19) to achieve convergence in the velocity distribution or transport properties. In Figure 11, we display the error in the two-term approximation ($l_{\max} = 1$) and the converged multi-term result. In the gas and liquid phases we see that the two-term approximation is sufficient to ensure accuracy to within 0.5% in the drift velocity, however errors as large at 10% are present in the characteristic energy. This indicates a failure of the two-term approximation for the evaluation of the characteristic energy. Similar findings in the gas-phase were found by Brennan and Ness [43]. Theories that have used the two-term approximation to iteratively adjust cross-sections may produce cross-sections that are inconsistent with a multi-term framework.

In Figure 11 we also consider the impact of anisotropic scattering on the validity of the two-term approximation. The two-term approximation can only sample the momentum transfer cross-section. Higher-order spherical harmonic components of the distribution function in expansions (19) are coupled to, and hence sample, higher-order coefficients in the expansion of the differential cross-section (see e.g. equation (31)). In Figure 11 we highlight
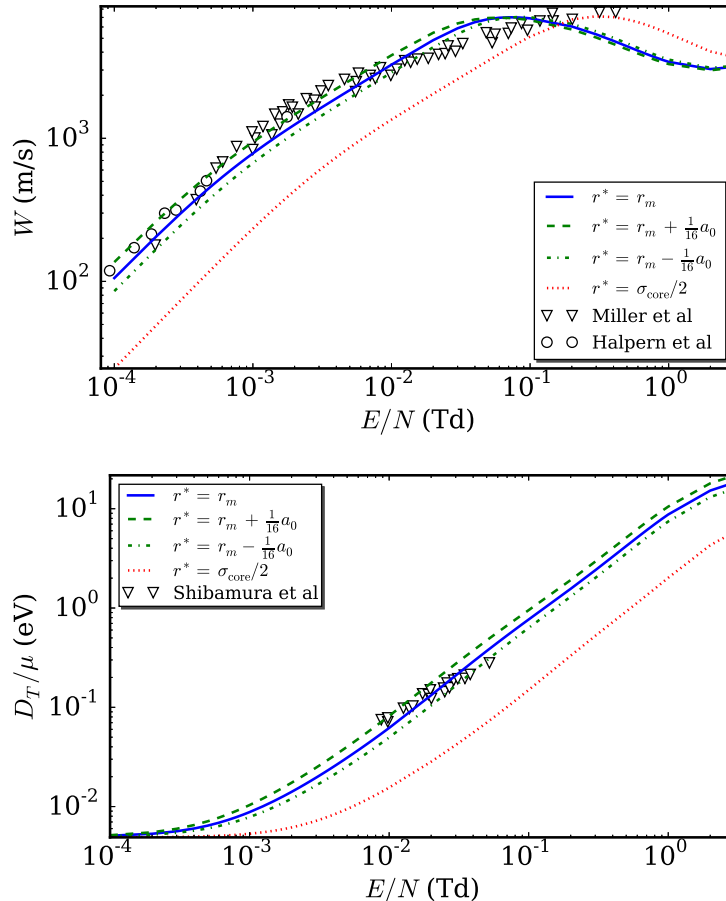
25

Figure 9. Comparison of the calculated drift and characteristic energy with variation in the distance r^* at which the phase shifts are determined. Experimental data is as detailed in Figure 7.

the differences, using dashed lines, between the multi-term approximation using only the momentum transfer cross-section (i.e. we assume $\sigma_{l \geq 2} = \sigma_1$) and those where the full differential cross-section is considered. The differences are less than 1% (usually less than 0.1%) indicating the distribution function is not sufficiently anisotropic to couple in higher-order partial cross-sections. Equivalently, anisotropy in the differential cross-sections has only a minimal impact on the anisotropy in the velocity distribution function.

VII.   CONCLUSIONS

We have extended the approach of Lekner and Cohen [8, 9], overcoming some of its limitations, to calculate the effective cross-sections and transport properties of electrons in liquid argon. For the first time an accurate multipole polarisability in the electron-atom
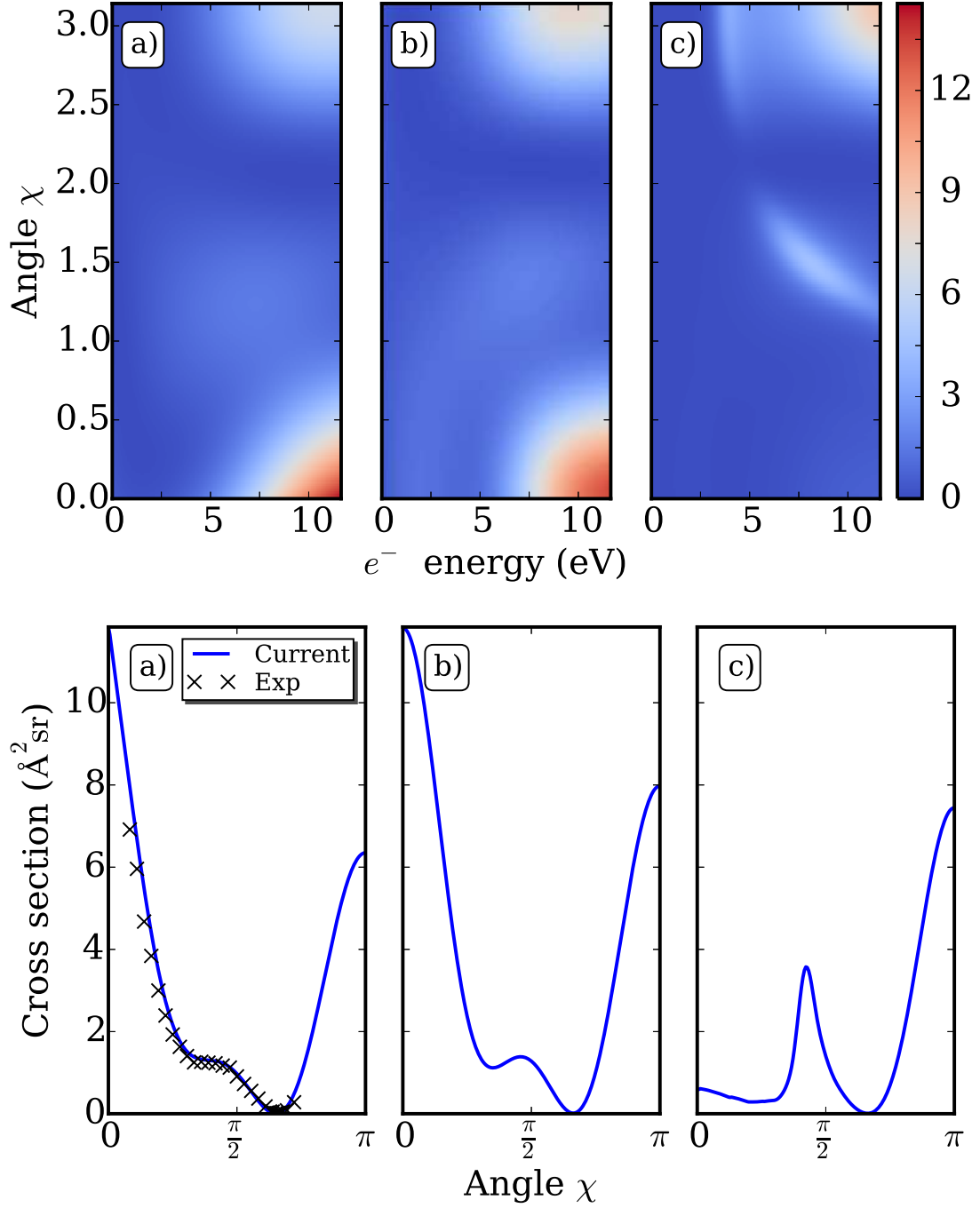
26

Figure 10. Top: Differential cross-sections in square angstroms per steradian for electrons in Ar for a) dilute gas phase, $\sigma(\epsilon, \chi)$ b) effective liquid phase including screening effects, $\sigma^{\mathrm{scr}}(\epsilon, \chi)$ and c) liquid phase cross-section including coherent scattering effects $\Sigma(\epsilon, \chi)$. Bottom: Differential cross-sections taken at 10 eV for the same cases. The experimental data for the gas phase is taken from Gibson et al. [42].
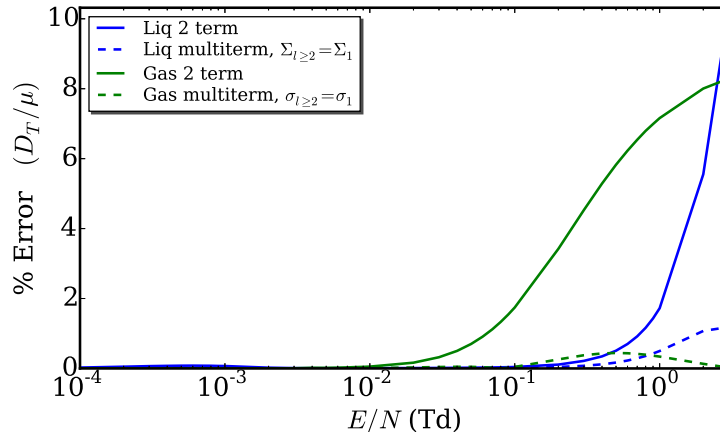
Figure 11. Percentage differences between the two-term and multi-term values of the characteristic energy for the gas and liquid phases using the full differentail cross-sections (solid lines), and percentage differences between the multi-term results with using only the momentum transfer cross-section and the full differential cross-section (dashed lines). All percentages are relative to the converged multi-term result using the full differential cross-section.

potential, and a fully non-local treatment of exchange were included in the calculation of liquid phase cross-sections using the full machinery of the Dirac-Fock scattering equations. The accuracy of the potential implemented and associated cross-sections calculated was confirmed by comparison with experiment in the gas-phase, and the importance of a fully non-local treatment of exchange was demonstrated. The result calls into question cross-sections (gas, liquid or clusters) which assume a local treatment of the exchange. Sensitivity to the radial cut-off for the electron-atom potential was presented, and while the maximum in the potential was shown to be a suitable choice, enhanced accuracy may be achieved with an energy dependent choice of the cutoff.

The calculation of the drift velocity and characteristic energies were performed for the first time using a multi-term solution of Boltzmann's equation accounting for coherent scattering. The full anisotropy of the liquid phase-phase differential cross-section was considered including anisotropy arising from both the interaction and from the structure factor. The multi-term framework enabled an assessment of the sensitivity to this anisotropy in the differential cross-section and in the velocity distribution function. While the two-term approximation was found to be sufficient for accuracies to within 1% for the drift velocity, errors of the order of 10% or more were found in the characteristic energy. The latter was

found to be the dominant contribution to the differences in the two and multi term results. It was found that both coherent scattering and screening of the electron-atom potential are required to reproduce the measured transport coefficient values. We emphasize that there are no free parameters in the current theory and its implementation, and hence the high level of agreement between the calculated and measured transport coefficients yields confidence that the essential physics has been captured in the theory.

VIII.   ACKNOWLEDGEMENTS

[1] P. Bruggeman and C. Leys, J. Phys. D **42**, 053001 (2009).

[2] M. G. Kong, G. Kroesen, G. Morfill, T. Nosenko, T. Shimizu, J. van Dijk, and J. L. Zimmermann, New J. Phys. **11**, 115012 (2009).

[3] W. Tian and M. J. Kushner, J. Phys. D **47**, 165201 (2014).

[4] S. A. Norberg, W. Tian, E. Johnsen, and M. J. Kushner, J. Phys. D **47**, 475203 (2014).

[5] C. Chen, D. X. Liu, Z. C. Liu, A. J. Yang, H. L. Chen, G. Shama, and M. G. Kong, **34**, 403 (2014).

[6] A. F. Borghesani, IEEE Transactions on Dielectrics and Electrical Insulation **13**, 492 (2006).

[7] G. Braglia and V. Dallacasa, Phys. Rev. A **26**, 902 (1982).

[8] M. H. Cohen and J. Lekner, Physical Review **158**, 305 (1967).

[9] J. Lekner, Physical Review **158**, 103 (1967).

[10] Y. Sakai, J. Phys. D **40**, R441 (2007).

[11] V. M. Atrazhev and I. T. Iakubov, J. Phys. C **14**, 5139 (1981).

[12] V. Atrazhev, I. Iakubov, and V. Pogosov, Phys. Lett. A **204**, 393 (1995).

[13] V. M. Atrazhev and I. V. Timoshkin, Phys. Rev. B **54**, 252 (1996).

[14] V. M. Atrazhev and I. V. Timoshkin, IEEE Trans. Dielectr. Electr. Insul. **5**, 450 (1998).

[15] R. A. Buckingham, Proc. Roy. Soc. London A **168**, 264 (1938).

[16] R. D. White and R. E. Robson, Phys. Rev. E **84**, 031125 (2011).

[17] R. D. White, R. E. Robson, B. Schmidt, and M. Morrison, J. Phys. D **36**, 3125 (2003).

[18] S. Chen, R. P. McEachran, and A. D. Stauffer, J. Phys. B **41**, 025201 (2008).

[19] R. P. McEachran, D. L. Morgan, A. G. Ryman, and A. D. Stauffer, J. Phys. B **10**, 663 (1977).

[20] R. P. McEachran and A. D. Stauffer, J. Phys. B **23**, 4605 (1990).

[21] D. J. R. Mimnagh, R. P. McEachran, and A. D. Stauffer, J. Phys. B **26**, 1727 (1993).

[22] A. Dorn, A. Elliot, J. C. Lower, S. F. Mazevet, R. P. McEachran, I. E. McCarthy, and E. Weigold, J. Phys. B **31**, 1127 (1998).

[23] L. S. Frost and A. V. Phelps, Phys. Rev. **136**, A1538 (1964).

[24] S. Buckman, J. W. Cooper, M. T. Elford, and M. Inokuti, in *Photon and Electron Interactions with Atoms, Molecules and Ions*, edited by Y. Itikawa (Darmstadt: Springer, 2003), vol. 17A, pp. 2–35.

[25] J. B. Furness and I. E. McCarthy, J. Phys. B **6**, 2280 (1973).

[26] B. H. Bransden and C. J. Noble, J. Phys. B **9**, 1507 (1976).

[27] R. P. McEachran, A. G. Ryman, and A. D. Stauffer, J. Phys. B **10**, L681 (1977).

[28] J. Yarnell, M. Katz, R. Wenzel, and S. Koenig, Phys. Rev. A **7**, 2130 (1973).

[44] Note1, in the arrangement of (16), it is possible to precompute the innermost integral cumulatively once and use its values in a look-up table.

[30] L. Boltzmann, Wien. Ber. **66**, 275 (1872).

[31] K. Kumar, H. Skullerud, and R. Robson, Aust. J. Phys. **33**, 343 (1980).

[32] R. Robson and K. Ness, Phys. Rev. A **33**, 2068 (1986).

[33] R. D. White and R. E. Robson, Phys. Rev. Lett. **102**, 230602 (2009).

[34] A. Robertson, Aust. J. Phys. **30**, 39 (1977).

[35] R. W. Warren and J. H. Parker, Phys. Rev. **128**, 2661 (1962).

[36] *Laplace database*, accessed 29 January, 2015, URL `www.lxcat.net`.

[37] *Dutton database*, accessed 29 January, 2015, URL `www.lxcat.net`.

[38] J. S. Townsend and V. A. Bailey, Phil. Mag. **44**, 1033 (1922).

[39] L. Miller, S. Howe, and W. Spear, Phys. Rev. **166**, 871 (1968).

[40] B. Halpern, J. Lekner, S. Rice, and R. Gomer, Phys. Rev. **156**, 351 (1967).

[41] E. Shibamura, T. Takahashi, S. Kubota, and T. Doke, Phys. Rev. A **20**, 2547 (1979).

[42] J. C. Gibson, R. J. Gulley, J. P. Sullivan, S. J. Buckman, V. Chan, and P. D. Burrow, Journal of Physics B Atomic Molecular Physics **29**, 3177 (1996).

[43] M. Brennan and K. Ness, Il Nuovo Cimento D **14**, 933 (1992).

[44] Note1, in the arrangement of (16), it is possible to precompute the innermost integral cumulatively once and use its values in a look-up table.